ARTICLE

Carbon Fibre From Renewable Resources: The Role of Lignin Molecular Structure on its Blendability with Biobased Poly(Ethylene Terephthalate)

Received 00th January 20xx,
Accepted 00th January 20xx

DOI: 10.1039/x0xx00000x

Anne Beaucamp[a], Yan Wang[a,b], Mario Culebras[a] and Maurice N. Collins*[a]

Biobased poly(ethylene terephthalate) has been successfully blended with isopropyl alcohol fractioned hardwood organosolv lignin. The blend compatibility was analysed using Gibbs free energy calculation and confirmed by glass transition temperature measurements as well as morphological study. The obtained carbon fibres from this blend displayed a turbostratic carbon phase and their morphology exhibits a one phase smooth surface. The carbon yield of the blend was found to be improved by fractionation reaching values of ~ 40%. The chemical structure of lignin, most notably the amount of available aromatic hydroxyl groups, was critical for the success of this work. The high molecular weight fraction is enriched with aromatic hydroxyl groups that can crosslink as ether type bonds such as β-O-4 and β-5 bonds. When substituted to aliphatic hydroxyls in a modified lignin, the blend with BPET was found to be incompatible and produced a carbon fibre exhibiting two phases, low carbon yield and a low amount of turbostratic phase.

Introduction

Biopolymers are being actively investigated as an alternative to petroleum-based raw materials for both economic and environmental reasons. [1] Lignin is the second most abundant polymer from biomass with 70 million tons available worldwide in 2017 from wood pulping processes. [2] However, only 2% of extracted lignin is valorised into products such as dispersants, adhesives, surfactants or as antioxidants in plastics and rubbers while the rest is mainly used to produce energy. [3] Lignin is extracted from plant cell walls where it accounts for 10-30 % wt. The plant type impacts on the composition of lignin in the monolignols syringyl (S), guaiacyl (G) and p-hydroxyphenyl (H) which interlink through bonds including β-O-4, β-5, 5-5, 5-O-4 and β-β. [4] The phenolic structure of lignin makes it a unique bio-based candidate for replacing polyacrylonitrile (PAN) as a raw material to produce carbon fibres (CF). However, the origin of lignin has a strong impact on the final CF: Hardwood lignin, from angiosperm plant types has a higher S content which reduces the amount of crosslinking in the structure compared to the softwood (coniferous) therefore increasing their linearity and from human activities such as corn residue have been investigated as carbon fibre precursor. The abondance of hydroxycinnamate groups as well as the presence of H phenolic groups impacted on the processability of the material with high viscosity and poor thermal stability, leading the authors to modify the lignin and mask the phenolic groups to process the material [7] . The extraction method influences the purity and breaks of the crosslinkages in the lignin, therefore affecting its processability [6, 8] : the organosolv process offers high extraction yields with high purity and low ash content. Also, the technique cleaves β-O-4 crosslinkages by acid catalyzation, liberating phenolic groups. [4, 6] Currently the mechanical properties of lignin-based CF are lower that of PAN-based ones, with to date a reported tensile strength of 1.07 GPa and modulus of 82.7 GPa for lignin against up to 7 GPa tensile strength and 500 GPa modulus for PAN. [1, 8] The variety of crosslinkages available between the lignin units makes the material highly heterogeneous and thermally unstable. Therefore, decreasing the amount of OH groups available for crosslinking is currently investigated as a mean to improve the quality of a carbon fibre precursor. [9] Chemical modification in the form of methylation and oxypropylation has been investigated by Argyropoulos et al. to mask the phenolic groups and reduce the reactivity of the rate high molecular weight weight chains, to reduce polydispersity and improve chemical homogeneity. Solvent fractionation was found to be an efficient and inexpensive method to separate low molecular weight from high molecular weight lignin. [11-14] Extensive research on fractionation showed that the amount of hydroxyl groups and β-O-4 crosslinkages in the lignin can be tuned by separating the molecular weight fractions. [13, 15, 16] Fractioned lignin-based carbon fibres with mechanical properties close to commercial PAN-based CF have been successfully electrospinned by Li et al. [9] A fraction of kraft lignin was obtained using an enzyme-mediator system and

[a] Bernal Institute, University of Limerick, Limerick, Ireland
[b] College of Materials and Textiles, Zhejiang Sci-Tech University, Hangzhou, P.R.China
*Corresponding author: Dr Maurice N Collins (Maurice.collins@ul.ie)

Keywords: lignin; bioPET; blends; carbon fibre

Electronic Supplementary Information (ESI) available: [details of any supplementary information available should be included here]. See DOI: 10.1039/x0xx00000x

blended with PAN at a weight ratio of 1:1. The high molecular weight fraction was found to produce the fibre of higher quality. Finally, the most recent work from Li et al. established that kraft lignin treated by acidic precipitation with high aromatic hydroxyls and low aliphatic hydroxyls produces carbon fibres with an elastic modulus of 20.7 GPa. [17]

Blending lignin with a thermoplastic polymer is a strategy to improve the processability and quality of the precursor fibre. [5, 9, 18, 19] The blending candidate must be miscible with lignin i.e. allows for strong interactions with the lignin chains. Poly(Ethylene Terephthalate) (PET) [20], Poly(Ethylene Oxide) (PEO) [21, 22] and most recently Thermoplastic Poly(Urethane) (TPU) [23] were found to successfully blend with hardwood lignin to produce homogeneous carbon fibres while Poly(Lactic Acid) (PLA) was found immiscible with lignin, forming porous carbon fibres. [24, 25] Among them, PET is widely used as a commonly plastic material. Only 60% of PET bottles and containers were recycled in the European Union in 2016 while the rest is left to pollute the surface of the planet and our oceans. Currently, a 30% plant-based bio-based PET is used for bottle packaging by food distribution companies. [26, 27] Blends of PET and lignin have been spun by electrospinning (50% lignin) [28] and melt-spinning [20] (75% lignin). The melt spun fibres were processed at temperature up to 265ºC and have a reported carbon yield of 38%. [20] However, there is a complete lack of understanding on how PET interacts with different types and fractions of lignin. The current authors have shown that a fundamental understanding of lignin chemistry throughout the carbon fiber process is key in order to produce high quality carbon fibers, as an understanding of the structure/property relationships involved in the blending process will enable targeted processing and predictable carbon phase formation. [29]

This work studies bio-based PET blended with different lignins (organosolv, fractionated organosolv and modified kraft) to provide a complete understanding of the process involved during carbon fibre production. The properties of the obtained lignins are evaluated using structural characterisation and thermal analysis. The impact of the hydroxyl groups of lignin on the miscibility with bio-based PET was evaluated using the Gibbs free energy of the blend. In addition, the use of both lignin and bio-based PET is expected to have a positive impact on the sustainability of carbon fibre production and to offer a new application field bio-based PET.

Experimental

Materials Organosolv Alcell Hardwood Lignin (OHL, Mw=3950 g.mol^{-1}, PDI = 4.7) and hydroxypropyl modified lignin (Mw=11357 g.mol^{-1} and PDI = 4.58) (ML) were supplied by Tecnaro (Ilsfeld, Germany as we previously reported. [22, 28] Bio-based Poly(terephthalate) (BPET, 30% Bio-MEG and 70% petro-based PTA) were manufactured by Honam Petrochemical Corp (Korea) and supplied by Tecnaro in pellets form.

Fractionation 60g of OHL was suspended in 1L of 2-propanol and left to stir for 24 hours. The insoluble part was filtered on grade 3 paper (Whatman, UK) and washed further with 2-Propanol. The solids were left to dry in the fume hood overnight before being placed in a vacuum oven at 55ºC for 24 hours. The weight of the fractioned lignin (FL) was measured and used to calculate the fractionation yield. When suspended in isopropanol, the lignin was partially dissolved. The yield of the fractionation was of 56% for the insoluble fraction.

Fibres Preparation OHL and FL powder were mixed with Bio-PET at various ratios using a 15 mL Micro compounder (Xplore) fitted with a 1.5mm diameter die at a screw speed of 150 rpm. Temperatures were determined according to the DSC and rheology results and are shown in Table 1. The extrude was then pelletised. The melt spinning was performed starting from pellets with the same speed and temperatures through a die with diameter 200 µm.

Thermal treatment Prior to carbonisation the fibres were stabilised in air at a ramp of 0.1ºC/min until 250ºC, with an isothermal treatment at 250ºC for one hour. Samples were carbonised in a quartz tube in nitrogen atmosphere at 1000ºC for 30 minutes using a heating rate of 10ºC/min.

Size-exclusion chromatography (SEC) was performed on an Agilent 1260 infinity GPC system with refractive index detector. As stationary phase, a PolarSil linear S column from PSS Polymer Mainz was chosen while the mobile phase was dimethylacetamide (DMAc) with the addition of LiBr (5 g/L) according to the method of Clauss et al. [21] Measurements were conducted at 50 °C and 0.75 mL/min and evaluated by conventional calibration against PMMA.

True Density measurements for the miscibility study were done using an AccuPyc II 1340/ Gas Pycnometer working with Helium. 2 to 3 grams of each samples were used and 10 measurements cycles were performed. The standart deviation is of 0.5 kg.m^{-3} for each density value.

Structural analysis of the samples before and after fractionation was performed using Fourier Transformed InfraRed (FTIR) transmission spectroscopy (PerkinElmer Spectrum 100 FTIR Spectrometer, USA) in the ATR mode in the range of 4000-650 cm^{-1} with a 1 cm^{-1} resolution. Each spectrum was taken with 10 repetitions. The solid state nuclear magnetic resonance (SS-NMR) was carried out on carbon 13 nuclei, Solid-state NMR data were acquired on a Bruker Avance III HD wide bore NMR spectrometer operating at a static magnetic field strength of B_0 = 9.4 T. Powdered samples of OHL, FL and ML were packed into 4 mm o.d. zirconia rotors with either Kel-F or zirconia caps. Carbon-13 NMR spectra were acquired under magic angle spinning (MAS) conditions using a Bruker 4 mm triple resonance (X/Y/1H) MAS probe operating in double resonance mode. Spectra were acquired at 13C and 1H Larmor frequencies of ν0 = 100.6 and 400.1 MHz, respectively, and processed using TopSpin version 3.5pl7. NMR spectra were acquired at temperature of 20C. Carbon-13 NMR spectra were collected using single pulse high-power decoupling with magic angle spinning (HPDEC-MAS) sequence. Samples were spun at MAS rates of 12 kHz. Carbon 90° pulses were 3 µs in length. Proton decoupling was carried out using the SPINAL64 [30] at a frequency of 83 kHz and was set at 7.8 µs in length and a power of 41 W. Recycle delays were set at 100s and 1536 scans were taken over 9 hours. Contact times in CP experiments were of 2 ms. Carbon-13 chemical shift values were referenced to TMS

at δ = 0 ppm by adjusting the field such that the methylene peak in the and proton decoupling 90 and 180° pulses were 4 and 8 µs in length, respectively 13C NMR spectrum of solid adamantane resonated at δiso = 38.48 ppm [31]. For all 13C NMR spectra, 10 Hz of line broadening was applied before processing.

Rheology The rheological measurements were carried out in a Discovery Hybrid Rheometer (DHR-2) from TA Instruments using a parallel geometry with disposable aluminium plates (25 mm diameter plate). A temperature sweep was done between 210°C to 255°C using an angular frequency of 10 rad/s. The lignin powder was heated until the experimental temperature leaving a gap of 1 mm between plates.

Thermal Analysis The glass transition temperature (Tg) of the lignin before and after fractionation was determined using Differential Scanning Calorimetry measurements (DSC 6, Perkin Elmer, USA) in nitrogen flow at 60ml/min. The powder samples were dried in a vacuum oven for 24 hours at 60 °C and 7.0 ± 0.5 mg of sample was packed in a sealed Aluminium pan. The sample was heated to 220 °C at 10 °C per minute to remove thermal history, cooled to 30 °C at 10°C per minute and heated to 270 °C at a heating rate of 10 °C per minute as described in [32]. Tg was determined from the second heating curve using the Universal Analysis Software (Version 4.5A, Texas Instrument, USA). The FL-BPET and ML-BPET blends were prepared by weight fraction and compounded in the twin screw extruder as described above. OHL-BPET blend could not be compounded due to the high extrusion temperature. The glass transition temperature of the blend was determined as for the lignins. The crystallinity χ of BPET in the blends was determined using the following equation [33] :

$$\chi = \frac{\Delta H_f - \Delta H_c}{\Delta H_f^o} * 100 \quad (1)$$

With ΔH_f and ΔH_c the enthalpy of fusion and crystallisation, respectively, in J.g^{-1} as measured by the Universal Analysis Software (Version 4.5A, Texas Instrument, USA) ; $\Delta H^o_{f100\%PET}$ the enthalpy standard of fusion for 100% crystalline PET, as $\Delta H^o_{f100\%PET}$ =140.1 J.g^{-1}. [34]

The potential carbon yield of the materials was determined using a SETARAM TG-DTA 1600 (Setaram Instrumentation, France), using alumina crucibles. The samples were heated in nitrogen to 1000oC at a heating rate of 10 °C/min. The Carbon Yield was determined using the formula:

$$CY = \frac{m_{1000}}{m_0}.100 \quad (2)$$

The activation energy of thermal degradation (Ea) was determined using the Coats and Redfern method [35], with a reactional order for lignin degradation of 1.0 as reported by [36]. The derived equation from the rate of decomposition of solid materials with an order of reaction of 1 is as below,

$$ln\left(\frac{-ln(1-\alpha)}{T^2}\right) = C - \frac{E_a}{RT} \quad (3)$$

Where α is the mass conversion, $\alpha = \frac{m_0 - m(t)}{m_0 - m_{1000}}$ fraction of solids decomposed at time t.

T is the reaction temperature in Kelvin, R is the Universal Gas Constant (8.314 J.mol^{-1}.K^{-1}). For α < 0.3, ln(-ln(1-α)/T^2) vs. 1/T gives a straight line , with *-Ea/R* the slope of the line as reported in [37] and [38]. The linear fit of the curve was done between the temperature of onset of degradation to T_α = 0.3.

Analysis of the carbon phase: The Raman spectra of the carbon fibres were recorded at room temperature in backscattering configuration with a Raman spectrometer (Horiba, LabRAM 1A) equipped with 514 nm laser. The laser was focused to a spot-size of ~10 µm onto the CF surface using a 50× microscope objective (Olympus). To avoid sample damage, the laser power was limited to a few microwatts. All measurements were calibrated with the spectra of a silicon sample and the spectrometer was kept in the same position to avoid inaccuracy. The graphite particle size L_a was determined using the Tuinstra and Koenig equation [39] as follow:

$$L_a = C(\lambda)\left(\frac{I_D}{I_G}\right)^{-1} \quad (4)$$

With $C(\lambda)$ = 4.4 nm for a 514 nm laser radiation.

Results and discussion

The chemical structure of the lignins were analyzed with Fourier Transformed IR using a semi-quantitative method described in [29], where the aromatic skeleton vibration at 1514 cm^{-1} is used to normalise the absorbance of the signals, allowing for comparison of each sample (Figure 1 (a)). Therefore, the normalised signals show differences in intensities linked to the quantities of vibrating groups in the sample.

The broad resonance at 1700 cm^{-1} is assigned to conjugated aldehydes and carboxylic acid groups. Their concentration is slightly reduced in FL, which is attributed to low hydrogen bonding capability for IPA. [12] This low hydrogen bonding capacity also impacts the concentration of aromatic hydroxyl (resonance at 1370 cm^{-1}) as the fraction is enriched in phenolic groups. ML presents resonances that are linked to the presence of G moieties, at 1268, 1154 and 1140 cm^{-1}, for C-O vibrations in the G aromatic ring, for C=O deformations in conjugated ester groups and for C-H aromatic in-plane deformations, respectively. The weak resonance at 1112 cm^{-1} implies that FL is richer in aromatic C-H than ML while the strong resonance at 1458 cm^{-1}, assigned to aromatic methyl groups shows increased substitutions on the aromatic ring for the fraction in comparison to the pristine lignin. Also, FL is enriched in ether groups (1212 cm^{-1}) in comparison with ML which is characteristic of β-O-4 or β-5 linkages. Finally, ML has a lower concentration of aromatic OH (resonance at 1370 cm-1) but a higher amount of aliphatic OH than OHL and FL which have a similar amount of aliphatic OH.

Figure 1 (b) displays the ^{13}C CP/MAS solid state NMR for OHL, FL and ML. The spectrum for OHL is typical of a hardwood lignin. The aromatic ring resonates at 148, 134, 105 and 55 ppm with respectively carbons 4,1 and 6 in the etherified aromatic ring for syringyl and aromatic methoxy groups. The aliphatic chains resonate at 173 ppm with carbonyl groups, 30 ppm for alkyl CH_2,

and 14 ppm for the end of chains CH_3. ML shows different signals that confirm the nature of the chemical modification. The resonances at 73, 66 and 18 ppm are assigned to carbons C_I, C_{II} and C_{III} of the hydroxypropyl aliphatic chain as shown Figure S1 of the supporting information file. Terminal methyl groups in aliphatic chains have their resonance below 17 ppm. The electronegativity of the hydroxyl in the hydroxypropyl group increases the displacement for the methyl group. The 66 ppm resonance is linked to the secondary alcoholic carbon and the 73 ppm to the carbon linked to the ether group. The aromatic ring of ML displays NMR signals at 132, 122 and 112 ppm for the carbons 4, 1, 6 and 2 respectively. These signals are typical of a guaiacyl rich lignin. FL displays a similar spectrum to OHL in the aromatic region, as the solvent treatment did not affect the chemical bonds of the phenyl unit. A new resonance is found at 64 ppm, characteristic of ether units and assigned to the C_γ in β-5 units as reported by Jiang et al. [16] for high molecular weight fraction. The signal at 24 ppm is attributed to alkyl CH_2, from lignin side chains.

As shown in figure S2 of the supplementary information file OHL, FL and ML display thermoplastic behaviour. The significant rise in Tg between OHL and FL is attributed to the elevation of molecular weight for the insoluble fraction (Table S1 of the supporting information). [12] The insoluble fraction presents an increased polydispersity index (PDI) which is typical of insoluble fractions of lignin. This increased PDI translates into a complex 3D structure for the high molecular weight fraction. The modified kraft lignin has a lower Tg than that of FL. This implies that the macromolecular chains of ML have higher mobility than that of FL. All lignins degrade at temperatures above 230°C.

The study of the evolution of the flow with varying temperature for OHL, FL and ML is displayed in Figure 2. The lignins display differing behaviours upon heating. The viscosity of pure OHL is low at 200°C and diminishes gradually across the temperature range, this is attributed to the higher degree of molecular mobility when temperature increases. It shows elastic behaviour across the temperature range with Tan(δ) below 0.5. Whilst FL and ML display a U-shaped profile for complex viscosity. This effect is attributed to π-stacking of the aromatic rings, reported for high molecular weight lignins. [10] At low temperatures these lignins show a chain alignment, which translates into high viscosity for temperatures below 205°C for ML and 240°C for FL. As the temperature increases the mobility of the chains increases as crosslinking is hindered by stacking of aromatic rings, until they eventually crosslink and the viscosity of the material increases, from 225°C for ML and 246°C for FL. FL shows a dampening effect and behaves as a liquid over the range of the precursor fibre processing temperature, while ML has an elastic behaviour that strengthens at temperatures above 225°C, as its complex viscosity increases while the dampening effect decreases below 0.25.

When lignin is blended with BPET the complex viscosity increases. OHL-based blends present strong thermal stability and a decrease of viscosity from 230°C is due to the melting of BPET. As the proportion of BPET increases in the blend, the viscosity decreases at a faster rate due to increased amount of melting BPET above 230°C. The onset of crosslinking for FL-BPET happens at 228°C for 25% of BPET and 221°C for 30% of BPET which suggests strong interaction between the crosslinked chains of BPET and FL, as reported previously for thermoplastic poly(urethane) [23]. The fractionation affects the viscosity of the blends across the temperature range as their viscosity is higher than that of OHL blends. On the other hand, the onset of crosslinking mechanisms is delayed by the presence of BPET in the ML blends (217°C for ML, 225°C for ML-BPET 75-25 and 237°C for ML-BPET 70-30), as lower interactions and higher amount of BPET hinders the crosslinking of ML. Blended FL shows lower viscosity and better thermal stability than ML for the 75-25% compositions around the processing range. When increased to 30%, BPET increases the viscosity for the three blends, rendering that composition or any further too viscous for extrusion. All the OHL and ML blends present an elastic behavior throughout the entire temperature range as tan(δ) is below 1. The damping effect for OHL increases after 235°C which suggests strong interactions between OHL and the BPET chains. Whilst, the damping of ML blends decreases above 236°C indicating weaker molecular interaction.

The DSC analysis for FL and ML blends are presented Table 2. When blended with BPET ML presents two glass transitions. The temperatures of glass transitions for ML-BPET blends stay constant regardless of composition, with Tg_1 attributed to BPET-rich phase and Tg_2 attributed to the ML-rich phase. These results suggest that the modification of lignin inhibits its miscibility with BPET and this is due to restricted π stacking and increased intramolecular hydrogen bonding within the ML chains. The fraction-based blend presents only one glass transition, of that the temperature is increased by up to 27°C for the 65% FL blend. This effect has been reported by these authors for lignin blended with thermoplastic elastomeric polyurethanes in [23] and was attributed to the hindering of lignin chain movement by the blended biopolymer. Also, the decrease of melt temperature is not as pronounced for ML blends as it is for FL blends at respective ratios, meaning higher interaction between the BPET and the fractioned lignin.

The crystallisation exotherm is not present in both blends at any composition. This behaviour has been reported for PET-PEI blends at composition below 50% PET. [40] The measured degree of crystallinity of the BPET is below 16% for both blends, with a slight increase for ML based blends in comparison with that of FL based blends, especially for compositions of 70% lignin and above. This effect is attributed to the presence of long aliphatic chains in ML that hinders hydrogen-type bonding and reduces the interaction between lignin and BPET chains, allowing the BPET chains to arrange themselves in an orderly manner. The Gibbs free energy can be determined to evaluate miscibility of the lignins and BPET. A negative Gibbs free energy of mixing is necessary for polymers to be miscible such as:

$$\Delta G_m = \Delta H_m - T\Delta S_m;\ \Delta G_m < 0 \qquad (5)$$

For a two components system ΔH_m can be expressed as a function of the volume fractions φ_1 and φ_2 of the components [41], such as:

$$\Delta H_m = (\delta_1 - \delta_2)^2 \varphi_1 \varphi_2 V_S \qquad (6)$$

With V_S, Volume of the system and δ_1 and δ_2 the respective solubility parameters of the polymers, expressed in $(MJ.m^{-3})^{1/2}$ or $(MPa)^{1/2}$.

Given the second principle of thermodynamics, the entropy can only increase during mixing so $\Delta S_m > 0$. The magnitude of ΔS_m is governed by the specific interactions between the polymers and by their molecular weight. High molecular weight polymers present a low amount of random mixing therefore low mixing entropy. So $\Delta S_m \approx 0$.

Therefore, the condition for polymer miscibility with $\Delta G_m < 0$ is $\Delta H_m \approx 0$. This condition is found to be true when the solubility parameters of the polymers are close in value.

The solubility parameter can be estimated using the group contribution method, which was introduced by Small. [42] Each functional group has a contribution F_i to the total molar attraction of the polymer. F_i is defined as a function of the cohesive energy E_i and the molar volume V_i of a functional group by the equation *(7)*,

$$F_i = (E_i V_i)^{1/2} \quad (7)$$

With E_i in $J.mol^{-1}$, V_i in $m^3.mol^{-1}$ and F_i in $(J.m^3)^{1/2}.mol^{-1}$.

The solubility parameter δ of a polymer is calculated as follows:

$$\delta = \frac{\rho \sum n_i F_i}{M} \quad (8)$$

With ρ and M density of the polymer in $kg.m^{-3}$ and molar mass in $kg.mol^{-1}$ of a repeat unit, respectively and $\sum n_i F_i$ the sum of all the molar group contribution for a repeat unit, in $(J.m^3)^{1/2}.mol^{-1}$. [41]

The repeat units for OHL, FL, ML and BPET can be found in Figure 3.

Both OHL and ML are hardwood lignins, therefore the proportion of G and S units were considered to be equal. [43] The structure of OHL allows for crosslinking through the phenolic group, while the hydroxypropylation of ML hinders such crosslinkages by blocking the aromatic hydroxyl groups. So repeat units for OHL are mainly based on β-O-4 linkages and that of ML on β-β linkages. As the fractionation process has enriched FL in phenolic groups and ether linkages the fraction repeat unit is based on β-O-4 and β-5 linkages.

Details of the group molar attraction constant calculation can be found in Table S3. The solubility of FL, ML and BPET and the mixing enthalpy were calculated using (2) and (3) and are displayed in Table 3. The solubility parameters of all lignins are close to that of BPET, with the fraction the closest value.

The fractionation process was found to have improved the miscibility with BPET in comparison with the hydroxylation process, thanks to the increase of phenolic hydroxyls that allow for higher rate of hydrogen bonding with the BPET repeat units. The lowest enthalpy of mixing was obtained for FL-BPET blend at 75-25 at 0.09. The same blend ration for OHL has an enthalpy of mixing of 0.14. Such value was reported for miscible blends of lignin and biopolyamide. [44] On the other way the enthalpy of mixing of ML-BPET blend was increased to 0.64. This theoretical calculation correlates the experimental observations on the glass temperature, as FL is a compatible blend for BPET while ML is incompatible, and the rheology results that showed how higher molecular interactions were obtained for BPET blended with FL. The pyrolysis behaviour of the lignin is affected by both fractionation and modification. OHL has an early onset with two thermal events at 250°C and 300°C which are attributed to the loss of methane and methanol. [29, 45] FL is more thermally stable with an onset of 265°C and a maximum degradation temperature of 396°C. This increased thermal stability has been reported for fractionated lignin. [46] The fractionation process also increases carbon yield, this behaviour is attributed to the condensation of higher molar mass lignin chains. However, FL degrades over a larger range of temperature and presents two degradation events at 396°C and 480°C. The second event can be linked to secondary degradation [45], as the fraction is richer in highly branched polymer chains. The lower carbon yield for ML suggests that the thermally induced crosslinkages in OHL participate to the carbon phase, whereas the lower number of phenolic groups in ML reduces the possibility of crosslinkages. [29] When blended, thermostability of the BPET increases as shown by a higher temperature of degradation and an increased degradation rate. Whilst participating in the carbon phase to a lower extent, as also reported in [20].

Table 4 reports the values of E_a for the lignins and blends. OHL has an activation energy of 45 $kJ.mol^{-1}$ that is in accordance with reported data. [36, 37] When fractioned, the activation energy of thermal degradation increases to 49 $kJ.mol^{-1}$, which is in line with the increased temperature of degradation and thermal stability. It re-joins reported degradation processes for hyperbranched aromatic structure, as FL has a more complex and amorphous structure than OHL. [38] Similarly, ML has an increased **E_a** that is coherent with the delayed onset of degradation and can be linked to a more orderly structure due to reduced crosslinkages. [29] The degradation of both blends demands higher energy, as pure BPET has a high activation energy which is attributed to the cyclisation of its chains above 350°C as well as its crystallinity. [38, 47]

Both the modified lignin and the fraction were successfully processed at temperature up to 250°C before the thermal decomposition of the lignins began, as shown in Table 1. ML was found to be more easily processed, as its hydroxyl groups have been replaced by hydroxypropyl groups, therefore hindering the crosslinking as previously reported. [29] During the compounding and spinning processes, both ML and FL blended at 75-25% with BPET showed the best spinnability due to comparatively low viscosity and stable rheological behaviour in the processing temperature range. These blends also provided the best compatibility as SEM images of the FL-BPET precursor fibres show no phase separation as shown in Figure 4, which is agreement with the DSC study. The precursor fibres are cylindrical with a diameter of 195 ± 35 µm and no voids. The fibres retain their shape and size after thermostabilisation in air. [48] After carbonisation the fibres had a diameter of 120 ± 27 µm. Although, these carbon fibre diameters are large they can be easily reduced using routine drawing techniques. Critically, the cross section shows a smooth and homogenous surface, with no porosity. The precursor fibres made from ML-BPET blend present macro-phase separation which is in agreement with the DSC results and the predictive theory results. The precursor

fibres are cylindrical with a rough and irregular surface morphology. When stabilised, the biphasic system remains as the domains grow. Therefore, the carbonised fibre presents two distinct carbon phases, with voids and defects on the surface. Raman spectroscopy was used to evaluate the quality of the carbon phase of the carbonised fibres. The deconvoluted signal shows two peaks assigned to the D and G modes. The D band is a breathing mode of the aromatic ring that is not present in perfect graphite, meaning it is only present in disordered systems whereas the G mode represents the relative motion of sp^2 carbon atoms. [49] The D band is centered at 1343 cm^{-1} for both blends, while the G band centre is placed at 1588 cm^{-1} for FL based CF and at 1581 cm^{-1} for the ML based CF. Also, the ratio of the intensities of the D vs. G bands is lower for FL based CF than for ML based CF. These results are consistent to an increased turbostratic graphitic phase for FL in comparison with ML. [9, 49] Finally, the particle size of the graphite in FL based CF is higher than that of ML based CF (4 nm vs. 3.6 nm), meaning the fractionation was beneficial to the formation of the turbostratic phase.

Conclusions

The studied lignin types, OSL, FL and ML and their blends with bio-based thermoplastic materials polyethylene terephthalate (BPET) represent an important class of potentially useful and abundant raw materials for a variety of applications. Here, the analysis has concentrated on their utility as starting polymers to produce carbon fibre. As reported, for this application an understanding of the structure/property relationships during processing are critical.

The lignin structure, the amount of phenolic OH and crosslinkages within the structure, play a crucial role on the miscibility, spinnability of the blend and ultimately on the quality of the carbon phase of lignin-BPET based carbon fibres. FL lignin shows higher Tg, higher amount of hydroxyl groups and higher amounts of ether linkages, increasing the miscibility with BPET. In contrast ML lignin where the phenolic groups were substituted for aliphatic hydroxyl groups, depicts a lower interaction degree with BPET polymer chains rendering poor miscibility. The experimental results correlated well with solubility parameter δ calculations and Gibbs free energy calculations with both indicating better miscibility for FL lignin. This clearly is evidenced in the pyrolysis results. ML blend shows a heterogenous morphology and reduced quality of the carbon phase whilst the lignin fraction fibres present a turbostratic carbon phase with a smooth monophasic cross section. Its carbon yield is improved to 39%. Taken overall it is considered that these results demonstrate that the interactions of these two lignins, although superficially similar, follow significantly different paths at the molecular level when blended with BPET. This results in differences in carbon fibre morphologies which can ultimately be utilised to tailor mechanical properties and tune porosity levels depending on application. Overall, the mechanical properties of these fibres require optimisation in pilot facilities in order to achieve sufficient structural integrity.

Conflicts of interest

There are no conflicts to declare.

Acknowledgements

The authors would like to thank Dr. Mark Steinmann for performing the Size-exclusion chromatography measurements.

AB, MC and MNC acknowledge received funding from the BioBased Industries Joint Undertaking under the European Union's Horizon 2020 research and innovation programme under grant agreement No 720707.

References

1. D. A. Baker and T. G. Rials, *J. Appl. Polym. Sci.*, 2013, **130**, 713.
2. R. Orbis, personal communication.
3. S. Laurichesse and L. Averous, *Prog. Polym. Sci.*, 2014, **39**, 1266.
4. S. Constant, H. L. J. Wienk, A. E. Frissen, P. d. Peinder, R. Boelens, D. S. van Es, R. J. H. Grisel, B. M. Weckhuysen, W. J. J. Huijgen, R. J. A. Gosselink and P. C. A. Bruijnincx, *Green Chemistry*, 2016, **18**, 2651-2665.
5. W. Fang, S. Yang, X.-L. Wang, T.-Q. Yuan and R.-C. Sun, *Green Chemistry*, 2017, **19**, 1794-1827.
6. Q. Sun, R. Khunsupat, K. Akato, J. Tao, N. Labb, N. C. Gallego, J. J. Bozell, T. G. Rials, G. A. Tuskan, T. J. Tschaplinski, A. K. Naskar, Y. Pu and A. J. Ragauskas, *Green Chem.*, 2016, **18**, 5015-5024.
7. W. D. Qu, J. Liu, Y. Xue, X. W. Wang and X. L. Bai, *Journal of Applied Polymer Science*, 2018, **135**, 11.
8. A. A. Ogale, M. Zhang and J. Jin, *Journal of Applied Polymer Science*, 2016, **133**.
9. Q. Li, S. Xie, W. K. Serem, M. T. Naik, L. Liu and J. S. Yuan, *Green Chem.*, 2017, **19**, 1628-1634.
10. H. Sadeghifar, C. Cui and D. S. Argyropoulos, *Industrial & Engineering Chemistry Research*, 2012, **51**, 16713-16720.
11. H. Sadeghifar and D. S. Argyropoulos, *ACS Sustainable Chemistry & Engineering*, 2016, **4**, 5160-5166.
12. A. Duval, F. Vilaplana, C. Crestini and M. Lawoko, *Journal*, 2016, **70**, 11.
13. V. Passoni, C. Scarica, M. Levi, S. Turri and G. Griffini, *ACS Sustainable Chemistry and Engineering*, 2016, **4**, 2232-2242.
14. T. Saito, J. H. Perkins, F. Vautard, H. M. Meyer, J. M. Messman, B. Tolnai and A. K. Naskar, *ChemSusChem*, 2013, **7**, 221-228.
15. A. S. Jaaskelainen, T. Liitia, A. Mikkelson and T. Tamminen, *Industrial Crops and Products*, 2017, **103**, 51-58.
16. X. Jiang, D. Savithri, X. Du, S. Pawar, H. Jameel, H. M. Chang and X. Zhou, *ACS Sustainable Chemistry and Engineering*, 2017, **5**, 835-842.
17. Q. Li, M. T. Naik, H. S. Lin, C. Hu, W. K. Serem, L. Liu, P. Karki, F. Zhou and J. S. Yuan, *Carbon*, 2018, **139**, 500-511.

18. S. Sen, S. Patil and D. S. Argyropoulos, *Green Chem.*, 2015, **17**, 4862-4887.
19. S. Kubo and J. F. Kadla, *Macromolecules*, 2004, **37**, 6904-6911.
20. S. Kubo and J. F. Kadla, *J. Polym. Environ.*, 2005, **13**, 97.
21. J. F. Kadla and S. Kubo, *Composites Part A: Applied Science and Manufacturing*, 2004, **35**, 395-400.
22. Q. Yu, A. Bahi and F. Ko, *Macromolecular Materials and Engineering*, 2015, **300**, 1023-1032.
23. M. Culebras, A. Beaucamp, Y. Wang, M. M. Clauss, E. Frank and M. N. Collins, *ACS Sustainable Chemistry & Engineering*, 2018, **6**, 8816-8825.
24. M. Thunga, K. Chen, D. Grewell and M. R. Kessler, *Carbon*, 2014, **68**, 159.
25. S. Wang, Y. Li, H. Xiang, Z. Zhou, T. Chang and M. Zhu, *Composites Science and Technology*, 2015, **119**, 20-25.
26. E. Petcore, personal communication.
27. C. The Coca-Cola, personal communication.
28. E. Svinterikos and I. Zuburtikudis, *Journal of Polymers and the Environment*, 2017, **25**, 465-478.
29. M. Culebras, M. J. Sanchis, A. Beaucamp, M. Carsí, B. K. Kandola, A. R. Horrocks, G. Panzetti, C. Birkinshaw and M. N. Collins, *Green Chemistry*, 2018, **20**, 4461-4472.
30. B. M. Fung, A. K. Khitrin and K. Ermolaev, *Journal of Magnetic Resonance*, 2000, **142**, 97-101.
31. C. R. Morcombe and K. W. Zilm, *Journal of Magnetic Resonance*, 2003, **162**, 479-486.
32. J. Lisperguer, P. Perez and S. Urizar, *Journal of the Chilean Chemical Society*, 2009, **54**, 460-463.
33. I. Campoy, M. A. Gómez and C. Marco, *Polymer*, 1998, **39**, 6279-6288.
34. Athas, *Journal*, 1994, **Appendix 1**, 777-894.
35. A. W. Coats and J. P. Redfern, *Nature*, 1964, **201**, 68-69.
36. G. Jiang, D. J. Nowakowski and A. V. Bridgwater, *Thermochimica Acta*, 2010, **498**, 61-66.
37. R. Ebrahimi-Kahrizsangi and M. H. Abbasi, *Transactions of Nonferrous Metals Society of China*, 2008, **18**, 217-221.
38. A. Oroumei, B. Fox and M. Naebe, *ACS Sustainable Chemistry & Engineering*, 2015, **3**, 758-769.
39. F. Tuinstra and J. L. Koenig, *The Journal of Chemical Physics*, 1970, **53**, 1126-1130.
40. J. M. Martínez, J. I. Eguiazábal and J. Nazábal, *Journal of Applied Polymer Science*, 1993, **48**, 935-937.
41. J. E. Mark, *Physical properties of polymers handbook*, Springer, 2007.
42. P. A. Small, *Journal of Applied Chemistry*, 1953, **3**, 71-80.
43. F. G. Calvo-Flores, J. A. Dobado, J. Isac-García and F. J. Martín-Martínez, *Lignin and lignans as renewable raw materials: chemistry, technology and applications*, John Wiley & Sons, 2015.
44. R. Muthuraj, M. Hajee, A. Horrocks and B. Kandola, *International Journal of Biological Macromolecules*, 2019.
45. R. A. Fenner and J. O. Lephardt, *Journal of Agricultural and Food Chemistry*, 1981, **29**, 846-849.
46. G. Wang and H. Chen, *Separation and Purification Technology*, 2013, **120**, 402-409.
47. B. J. Holland and J. N. Hay, *Polymer*, 2002, **43**, 1835-1847.
48. E. Frank, L. M. Steudle, D. Ingildeev, J. M. Spörl and M. R. Buchmeiser, *Angewandte Chemie International Edition*, 2014, **53**, 5262-5298.
49. A. C. Ferrari and J. Robertson, *Physical Review B*, 2000, **61**, 14095-14107.

Figures

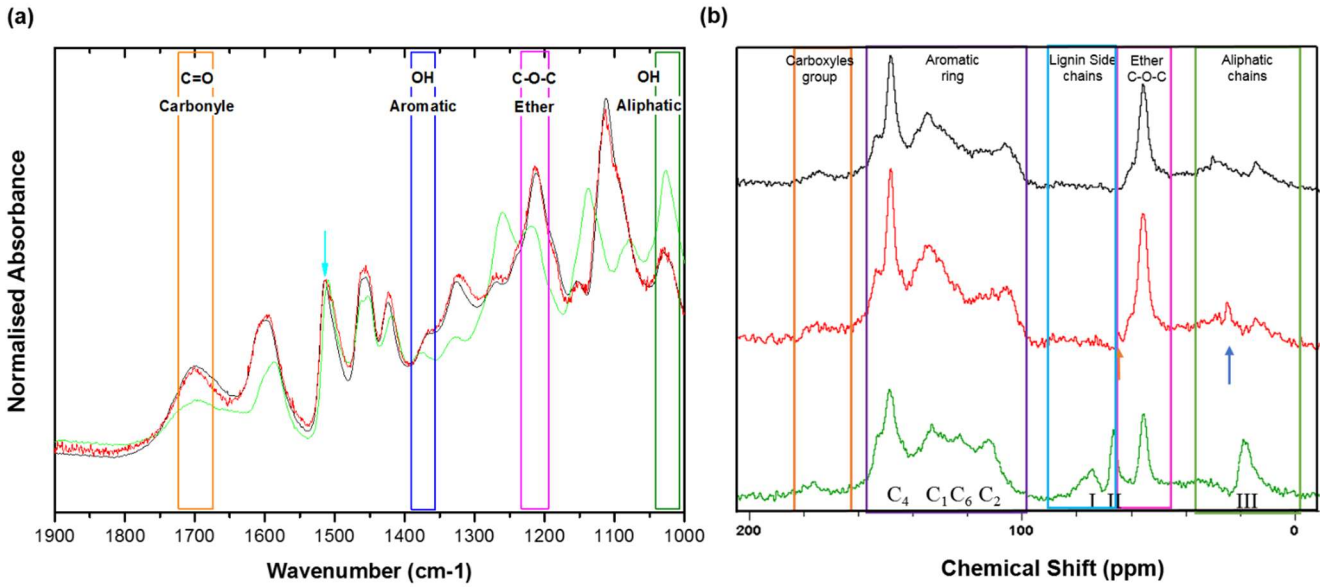

Figure 1: Chemical Analysis of OHL (black), FL (red) and ML (green). (a) represents the finger print area of the FTIR Spectra for the lignins. The intensities of the signals were normalised with respect to the intensity of the signal at 1514 cm-1, considered as an invariant band due to the aromatic skeleton of the lignins. [45] (b) represents the 13C Magic Angle Spin Solid State NMR for OHL (black), FL (red) and ML (green)

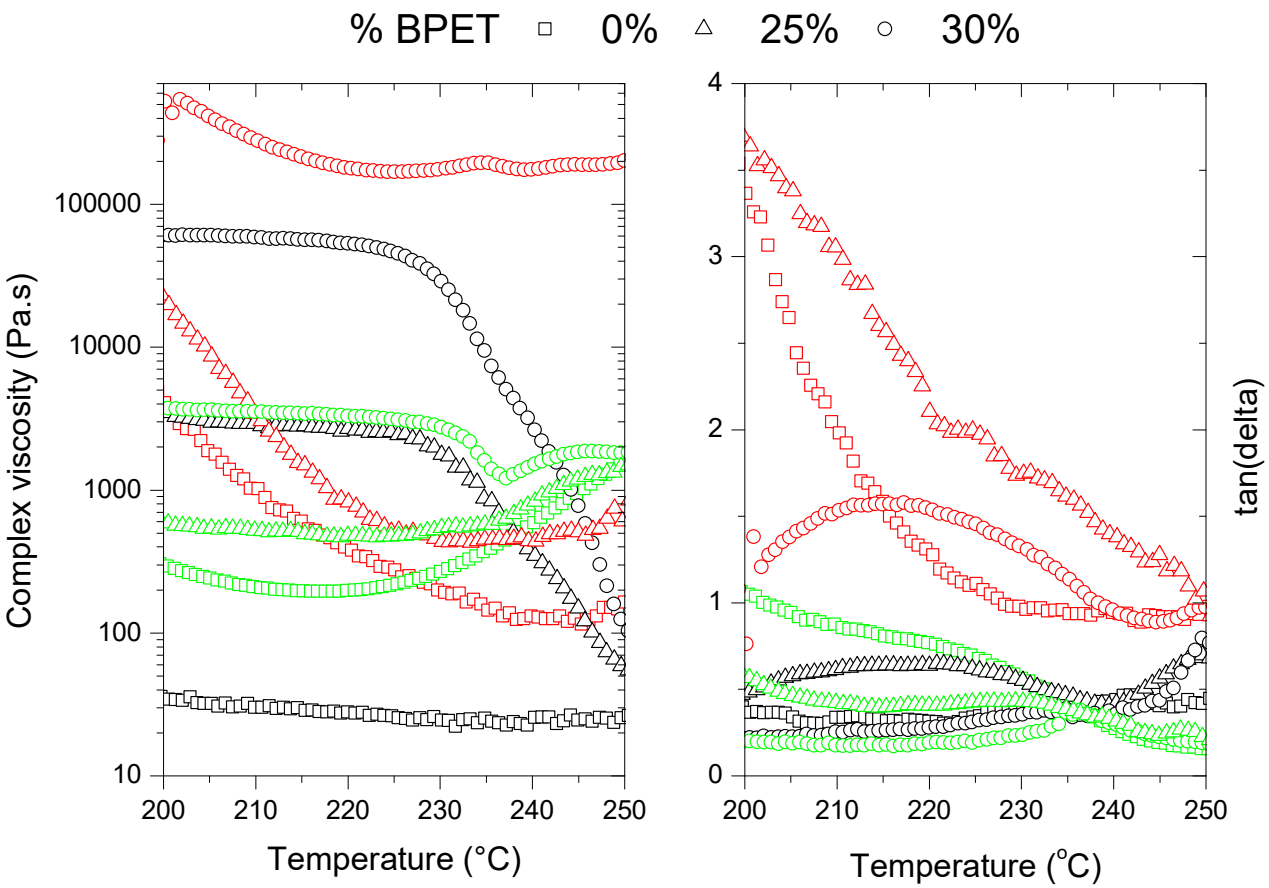

Figure 2: Evolution of the complex viscosity and tan(delta) as a function of temperature for OHL (Black), FL (Red) and ML (Green) pure and blended with BPET at Lignin-BPET 75-25% and 70-30%.

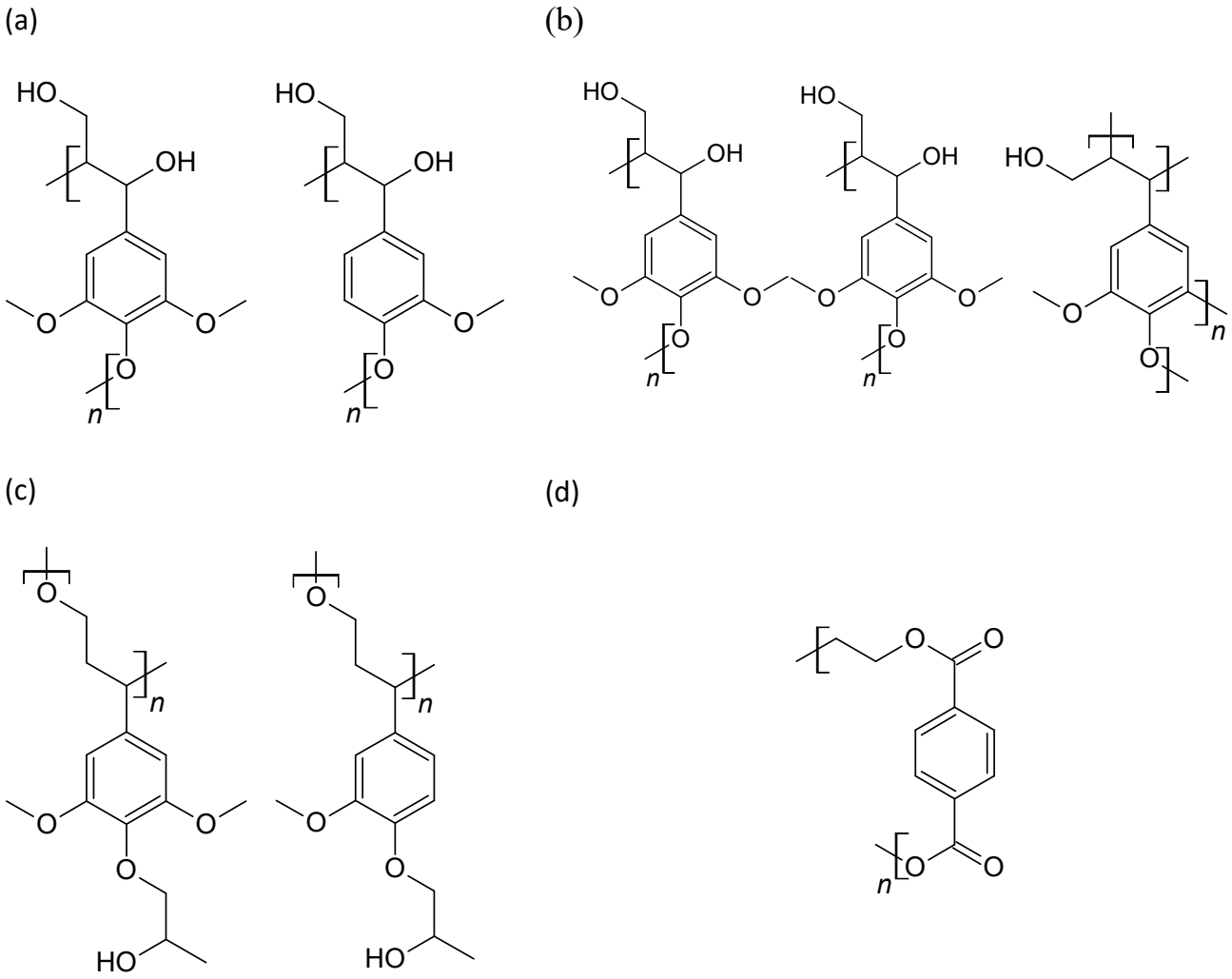

Figure 3: Proposed repeat unit for (a) OHL, (b) FL, (c) ML and (d) BPET

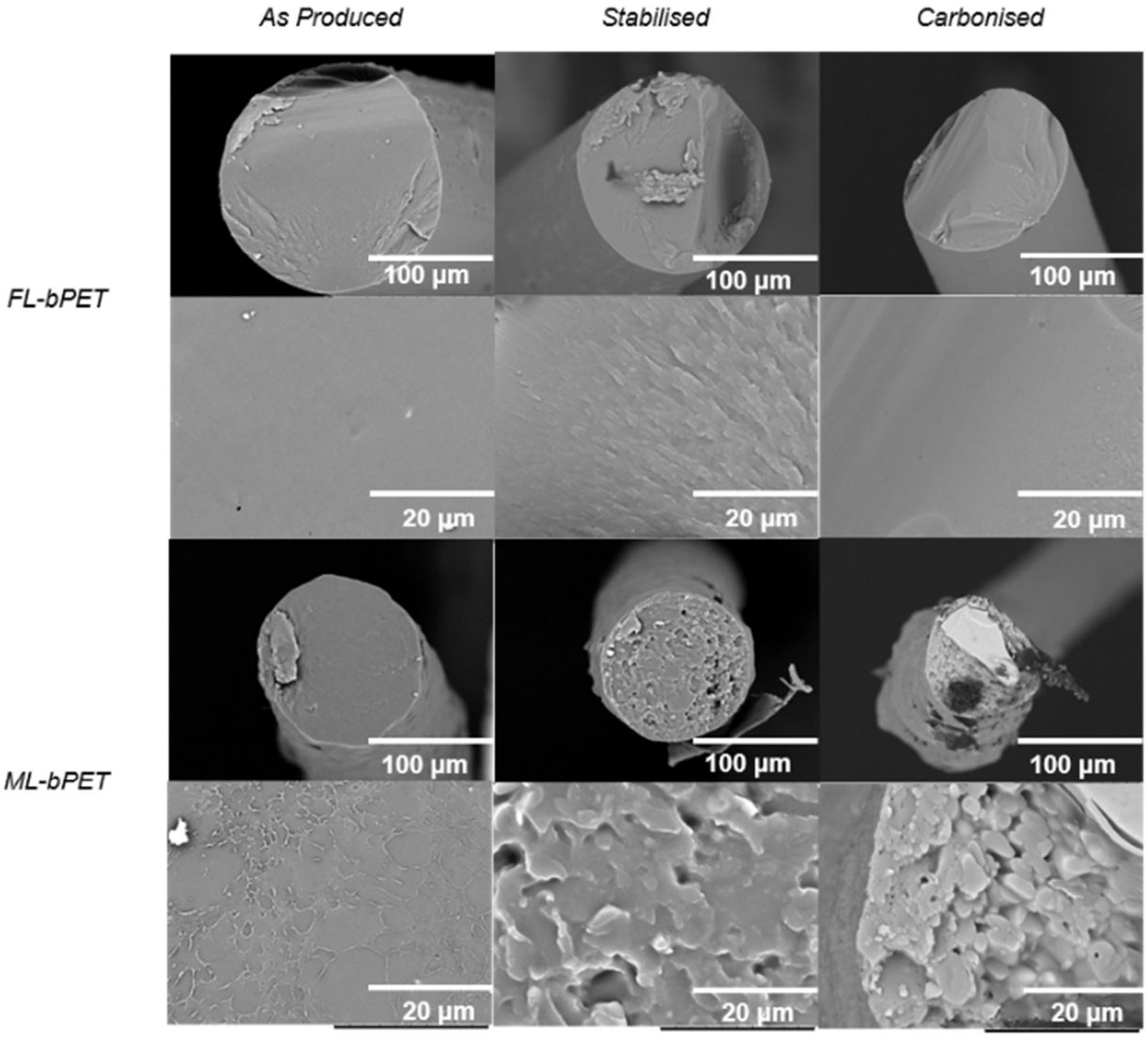

Figure 4: Micrographs of the precursor, stabilised and carbonised fibres for the FL-BPET 75-25 and ML-BPET 75-25 blends

Table 1: Processing temperature and spinnability of the Lignin-BPET blends at compositions varying between 80-20 to 65-35.

Sample Composition	OHL-BPET		FL-BPET		ML-BPET	
	Processing Temperature (°C)		Processing Temperature (°C)		Processing Temperature (°C)	
	Spinnability		Spinnability		Spinnability	
80-20	170-230-250	-	172-230-255	-	170-230-252	+
75-25	170-230-250	-	172-230-255	++	170-230-252	++
70-30	170-230-250	-	172-230-255	+	170-230-253	++
65-35	170-230-250	-	172-230-255	-	170-230-254	+

+ indicates spinnability

Table 2: Temperatures of Glass (Tg_1 and Tg_2), Melting transition (Tm) and crystallinity of BPET χPET for FL-BPET blends (a) and ML-BPET Blends (b)

(a)

% BPET	T_{g1} (°C)	T_{g2} (°C)	T_m (°C)	χ_{PET} (%)
0	-	150	-	-
20	-	171	240	7
25	-	163	243	9
30	-	164	242	9
35	-	177	240	16
100	81	-	253	28

(b)

% BPET	T_{g1} (°C)	T_{g2} (°C)	T_m (°C)	χ_{PET} (%)
0	-	116	-	-
20	87	127	246	9
25	81	125	247	11
30	87	125	248	11
35	85	125	250	16
100	81	-	253	28

Table 3: Solubility parameter and enthalpy of mixing for FL, ML and BPET blends

Samples	Density ρ (kg.m^{-3})	Group Molar Constant $\sum n_i F_i$ ((J.m^3)$^{1/2}$. mol^{-1})	Solubility Parameter δ (MPa$^{1/2}$)	Enthalpy of Mixing per unit of volume (J.m^{-3})
OHL	1325	6.9774	21.91	
FL	1342	9.8737	22.08	-
ML	1290	8.2062	20.92	-
BPET	1340	3.267	22.78	-
OHL/BPET 50-50 (%vol)	-	-	-	0.19
OHL/BPET 75-25 (%vol)	-	-	-	0.14
FL/BPET 50-50 (%vol)	-	-	-	0.12
FL/BPET 75-25 (%vol)	-	-	-	0.09
ML/BPET 50-50 (%vol)	-	-	-	0.86
ML/BPET 75-25 (%vol)	-	-	-	0.64

Table 4: Carbon Yield at 1000°C (CY), Temperature of Maximum Mass Loss (T_{max}) and Activation Energy for the thermal degradation (Ea) with corresponding R^2 values for the lignins and blends.

Lignin	0% BPET			25% BPET			100% BPET		
	CY %	Tmax °C	Ea (R^2) kJ.mol^{-1}	CY %	Tmax °C	Ea (R^2) kJ.mol^{-1}	CY %	Tmax °C	Ea (R^2) kJ.mol^{-1}
-							11	442	289 (0.998)
OHL	37	382	45 (0.994)	-					
FL	39	396	49 (0.9996)	33	391	78 (0.997)			
ML	34	396	54 (0.995)	34	400	86 (0.996)			